THE JOURNAL OF PHYSICAL CHEMISTRY A
A JOURNAL OF THE AMERICAN CHEMICAL SOCIETY

pubs.acs.org/JPCA

Article

Effective Phase Space Representation of the Quantum Dynamics of Vibrational Predissociation of the $ArBr_2(B,\nu = 16\cdots25)$ Complex

Juan Carlos Acosta-Matos, Christoph Meier, Aliezer Martínez-Mesa, and Llinersy Uranga-Piña*

Cite This: *J. Phys. Chem. A* 2022, 126, 1805−1815

Read Online

ACCESS | Metrics & More | Article Recommendations

ABSTRACT: We perform trajectory-based simulations of the vibrational predissociation of the $ArBr_2(B,\nu=16\cdots25)$ van der Waals triatomic complex, constrained to the T-shape geometry. To this aim, we employ a 2-fold mapping of the quantum dynamics into classical-like dynamics in an extended phase space. The effective phase space comprises two distinct sets of degrees of freedom, namely a collection of coupled harmonic oscillators and an ensemble of quantum trajectories. The time evolution of these variables represent bound and unbound motions of the quantum system, respectively. Quantum trajectories are propagated within the interacting trajectory representation. The comparison between the lifetimes of the predissociating complexes computed using the trajectory-based approach and the experimental results available for the target systems indicates that the present method is competitive with wavepacket propagation techniques. The competition between several simultaneous vibrational relaxation pathways was found to have a direct impact on the time scales of vibrational predissociation. Likewise, the analysis of the time evolution of the trajectories reveals the existence of regions in the effective phase space where transitions to vibrational states of higher energy are more likely to occur. The size and location of these regions influence the transient vibrational distributions and therefore the computed lifetimes. Furthermore, the mechanisms of energy redistribution along the dissociation coordinate are analyzed.

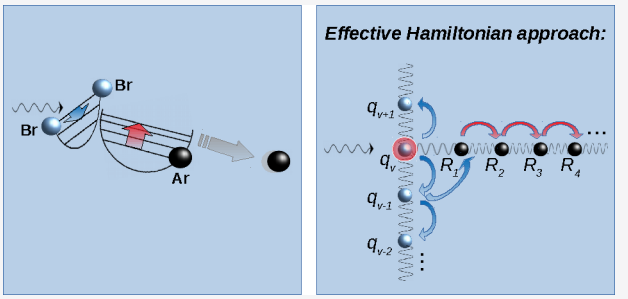

I. INTRODUCTION

In the past few decades, the continuous progress in time-resolved spectroscopic techniques has enabled the investigation of dynamical phenomena in atomic and molecular systems down to the femtosecond first, and more recently to the attosecond time scale. Likewise, modern computational modeling and simulation techniques, combined with state-of-the-art high-performance scientific computing technology, allow one to calculate the physical and chemical properties of systems composed of more than 10^{12} particles,[1−4] both for time-dependent processes and for systems in thermodynamic equilibrium. In general, essentially exact calculations (i.e., up to statistical errors associated with the total simulation time and the size of the simulation cell) are possible in physicochemical phenomena where the nuclear motion can be described classically.

Nonetheless, a similar accuracy is difficult to achieve for quantum systems with arbitrary chemical composition and structure. Theoretical and computational models allow one to translate the experimental signals into explicit representations of nuclear motion; therefore, continuous effort is made in order to develop new computational methods that can overcome these limitations (in situations where quantum effects on the molecular structure and dynamics are non-negligible).

Often, the performance of these computational tools varies strongly from one application to another, and some molecular systems have evolved as paradigmatic test systems for novel computational approaches and methodologies. Vibrational predissociation of van der Waals aggregates belongs in this class of model phenomena. As such, it has been extensively studied experimentally and investigated theoretically using fully quantum mechanical approaches.[5−28] Many of these investigations were devoted to gain a deeper understanding of the fundamentals of vibrational predissociation in triatomic dihalogen−rare gas complexes.[29−35]

In dihalogen−rare gas molecules, RgXY (Rg stands for the rare gas atom, XY is a homonuclear or heteronuclear dihalogen molecule), the vibrational predissociation usually consists of two main steps. First, the molecule undergoes vibronic excitation (from the ground electronic state) to a well-defined vibrational level ν of the dihalogen stretching mode, in the

Received: October 3, 2021
Revised: January 25, 2022
Published: March 14, 2022

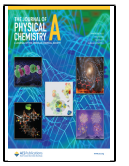

https://doi.org/10.1021/acs.jpca.1c08678
J. Phys. Chem. A 2022, 126, 1805−1815

electronic excited state of XY. In the following, we will consider the photoexcitation of the diatomic molecule into the electronic state B. The excess energy deposited by the optical excitation is initially localized in the dihalogen molecule, while the van der Waals mode remains in its ground vibrational state. Second, a radiationless transition takes place from the initially populated vibrational state ν to a lower vibrational level ($\nu' < \nu$) of the same electronic potential energy surface. Owing to the frequency mismatch between the diatomic molecule stretching mode and van der Waals vibrations, the intramolecular vibrational energy redistribution (i.e., the energy flow from the covalent bond into the weaker van der Waals bond) results in the fragmentation of the complex in rare gas and dihalogen fragments. Depending on the specific chemical species involved, the halogen molecule stretching mode may loose one or several vibrational quanta during the dissociation process.

Among the family of triatomic van der Waals aggregates, ArI_2 and $ArBr_2$ were found to exhibit a more intricate dynamics, e.g., with competition between the vibrational and electronic predissociation channels, the coexistence of discrete bands and a continuous spectrum, and the possible interference between different relaxation pathways depending on the specific vibrational level initially excited.[23,30,36] Another interesting feature is the possibility to discriminate experimentally between photoexcited linear and T-shape isomers, which undergo predissociation on quite different time scales.[23,30]

The limitations of modern wavepacket propagation techniques, regarding the simulation of vibrational predissociation of polyatomic van der Waals aggregates, have triggered the development of a variety of semiclassical approximations,[37−49] the application of the quasi-classical trajectory (QCT) method being the most prominent example. Semiclassical methodologies are often benchmarked against experimental results and quantum mechanical calculations for triatomic systems, and subsequently applied to larger aggregates.

Within the quasi-classical trajectory method, the time-dependent evolution of the system is represented by a swarm of classical trajectories, with initial conditions that sample the initial quantum mechanical state.[50−53] Although the effect of quantum delocalization is partially accounted for (via the initial distribution of trajectories in phase space), this approach neglects the influence of quantum effects on the subsequent dynamics.

Other alternatives have been employed to generate a trajectory representation of the dynamics (in an effective phase space) from the time-dependent Schrödinger equation, usually based on the Dirac−Frenkel variational principle (for instance, the Gaussian Wave-Packet method,[54,55] or the Quantized Hamiltonian Dynamics[56−58]). Conversely to the QCT method, the latter approaches allow one to partially incorporate quantum effects into the dynamical evolution of the system. Some treatments allow to incorporate higher-order quantum mechanical corrections perturbatively.[58,59] As another option, chemical reaction rates and diffusion coefficients can also be computed, in an extended phase space, using Ring Polymer Molecular Dynamics.[60]

A third family of methodologies aims to map the quantum dynamics *exactly* into a trajectory description. For instance, in refs 61 and 62, the time evolution of a quantum system is mapped into the motion of a set of coupled harmonic oscillators. This representation is similar in spirit to the Meyer−Miller model,[63] and it is well suited when the target process involves the population of a finite set of energy eigenstates. Likewise, the quantum trajectory method[64−67] translates the time-dependent Schrödinger equation into the time evolution of trajectories on an effective potential energy surface, resulting from the superposition of the interaction potential and the quantum potential. The latter is responsible for bringing all the quantum effects into the dynamics.

In particular, the parametric representation of the quantum potential introduced in refs 68 and 69, and its discretized version[70] generates a classical-like dynamics in a higher dimensional space, i.e., the *interacting trajectory representation* (ITR), which has been successfully applied to the description of ultrafast quantum dynamics.[71,72] Starting from the quantum Liouville equation rather than the time-dependent Schrödinger equation, a reminiscent of the ITR was introduced in ref 73. The latter is based on the propagation of the so-called entangled trajectories, which obey different equations of motion.

Both the classical mapping of refs 61 and 62 and the interacting trajectory representation have been combined into a single theoretical framework which yield promising results for the description of the vibrational predissociation of the Ar···Br_2(B,ν=24) T-shaped complex.[74] Opposite to previous QCT models of vibrational predissociation, this combined framework provides a fully quantum-mechanical, trajectory-based description of the dissociation dynamics. On the one hand, the trajectories represent the flow lines of the probability density along the reaction coordinate (i.e., the separation between the rare gas atom and the center of mass of the dihalogen molecule). On the other hand, for the bound motion (Br−Br stretching), the square amplitude of the oscillations (or equivalently, the energy of the oscillators) matches the occupation probability of the corresponding vibrational state. As the trajectory motion along the reaction coordinate is coupled to a set of classical-like harmonic oscillators, the present model has a clear connection to system−bath approaches commonly used in classical statistical mechanics.

The aim of this paper is to investigate the quantum dynamics of the vibrational predissociation of photoexcited $ArBr_2$(B,ν) van der Waals aggregates within the 2-fold mapping introduced in ref 74, for a wide range of initial vibrational states undergoing predissociation of the complex. Vibrational predissociation of $ArBr_2$ is chosen as target phenomenon since the availability of previous experimental and theoretical results[30] makes it an ideal benchmark for assessing the convergence properties, numerical accuracy and computational efficiency of the interacting trajectories methodology.

The paper is organized as follows. In section II, we present the main aspects of the phase space representation and the details of its numerical implementation. In section III, we present the results concerning the vibrational population dynamics and the mechanism of vibrational predissociation of the title system, and we discuss them in terms of the time evolution of the quantum trajectories. The conclusions are presented in section IV.

II. METHODS

II.A. Effective Phase Space Representation of the Vibrational Predissociation Dynamics. The quantum

https://doi.org/10.1021/acs.jpca.1c08678
J. Phys. Chem. A 2022, 126, 1805−1815

dynamics of the vibrational predissociation of the Ar···Br_2 complex in the B electronic state:

$$\mathrm{Ar}\cdots \mathrm{Br}_2(\mathrm{B},\ \nu) \rightarrow \mathrm{Br}_2(\mathrm{B},\ \nu' < \nu) + \mathrm{Ar} \tag{1}$$

for vanishing total angular momentum and for a fixed angle between the Jacobi vectors (e.g., at the equilibrium angular position), is mapped into an effective phase space dynamics governed by the classical-like Hamiltonian:

$$\mathcal{H} = \sum_{\alpha,\alpha'}\left[(\hat{H}_{\mathrm{Br}_2})_{\alpha\alpha'} + \frac{1}{N}\sum_i W_{\alpha\alpha'}(R_i)\right](q_\alpha q_{\alpha'} + p_\alpha p_{\alpha'}) + \frac{1}{N}\left[\sum_i \frac{P_i^2}{2\mu} + Q(R_1, ..., R_N)\right]. \tag{2}$$

The Hamiltonian (2) was derived within the time-dependent Hartree (TDH) approximation,[74] and it describes the time evolution of a set of N_α coupled, classical-like oscillators, q_1, q_2, ..., q_{N_α}, and a second set of N degrees of freedom R_1, R_2, ..., R_N (i.e., the interacting trajectories). The coupling between the two subsystems is described by the terms containing the quantities $W_{\alpha\alpha'}(R) = \langle\alpha|W(r, R)|\alpha'\rangle$. The latter are the matrix elements of the van der Waals interaction $W(r, R)$ between the Br_2 molecule and the Ar atom, computed in the basis of the eigenfunctions $|\alpha\rangle$ of the vibrational Hamiltonian $\hat{H}_{\mathrm{Br}_2}$ of the isolated dihalogen molecule. Hereafter, the variables r and R stand for the distance between the two Br atoms and between the Ar atom and the Br_2 center of mass, respectively.

The dihalogen−rare gas interaction in the ground electronic state X is modeled using a Morse−van der Waals function. The later is only used in the generation of the initial conditions for the quantum trajectories along the van der Waals mode, since the subsequent dynamics proceeds on the potential energy surface corresponding to the electronic state B. In the electronic state B, the interatomic interactions are represented using pairwise Morse potentials. The same parameters as in refs 74−76 were used for the Br−Br interaction potential and for the Br−Ar interatomic potentials building up the potential energy surface $W(r, R)$.

In eq 2, the term $(\sum_i P_i^2)/(2\mu N)$ represents the kinetic energy associated with the motion along the dissociation coordinate R, and $\mu = \frac{m_{\mathrm{Ar}} m_{\mathrm{Br}_2}}{m_{\mathrm{Ar}} + m_{\mathrm{Br}_2}}$ is the reduced mass corresponding to this displacement. Furthermore, $Q(R_1,...,R_N)$ represents the quantum potential for the motion along the van der Waals degree of freedom, evaluated within the interacting-trajectory representation framework.[74]

Moreover, q_α and p_α are effective generalized coordinates and their conjugate momenta, respectively. The quantity $|c_\alpha|^2 = \frac{1}{2}({q_\alpha}^2 + {p_\alpha}^2)$ defines the occupation probability of the different vibrational levels of the diatomic molecule (which is also the energy of the oscillator α), from which the lifetime τ of the initially excited level can be determined.

Inserting the notation $\mathcal{H}^{\mathrm{Br}_2}_{\alpha\alpha'} = (\hat{H}_{\mathrm{Br}_2})_{\alpha\alpha'} + \frac{1}{N}\sum_i W_{\alpha\alpha'}(R_i)$, the equations of motion read:

$$\begin{cases} \dot{q}_\alpha = \sum_{\alpha'} \mathcal{H}^{\mathrm{Br}_2}_{\alpha\alpha'} p_{\alpha'}, \\ \dot{p}_\alpha = -\sum_{\alpha'} \mathcal{H}^{\mathrm{Br}_2}_{\alpha\alpha'} q_{\alpha'}, \\ \dot{R}_i = \frac{1}{\mu} P_i, \\ \dot{P}_i = -[f(R_i) + f_q(R_i)]. \end{cases} \tag{3}$$

In eq 3, $f(R_i)$ and $f_q(R_i)$ stand for the interaction force and the quantum force acting on the ith interacting trajectory, respectively. The (Bohmian) quantum force $f_q(R_i) = -\frac{\partial Q}{\partial R_i}$ is computed analytically in terms of the position of every quantum trajectory and its first and second nearest neighbors, using the following expression:[74]

$$f_q(R_i) = \frac{1}{4\mu}\left(\frac{1}{(R_{i+1} - R_i)^2}\left[\frac{1}{R_{i+2} - R_{i+1}} - \frac{2}{R_{i+1} - R_i} + \frac{1}{R_i - R_{i-1}}\right] - \frac{1}{(R_i - R_{i-1})^2} \times \left[\frac{1}{R_{i+1} - R_i} - \frac{2}{R_i - R_{i-1}} + \frac{1}{R_{i-1} - R_{i-2}}\right]\right).$$

The set of equations in eq 3 will be used to describe the time-evolution of the dihalogen−rare gas complex constrained to the T-shape geometry. This geometrical constraint is motivated by the possibility to discriminate between the T-shape and the linear isomers in femtosecond spectroscopy experiments of vibrational predissociation.[30] Albeit being represented as a well-defined trajectory in a 2 $(N_\alpha + N)$ -dimensional phase space, the present description of the vibrational predissociation dynamics is fully quantum-mechanical.

The predissociation lifetime is computed as the inverse of the rate of population of the final vibrational states, $|c_{\nu'}(t)|^2 = \frac{1}{2}({q_{\nu'}}^2 + {p_{\nu'}}^2)$, i.e., the total population P_{diss} of all open dissociation channels is assumed to behave exponentially ($P_{diss} = \sum_{\nu'} |c_{\nu'}|^2 \sim [1 - \exp\{-(t - \tau_0)/\tau\}]$), and possibly adding a time lag τ_0 (i.e., the time elapsed prior to the onset of the dissociation). Hence, τ measures the rate of appearance of the final products rather than the rate of disappearance of the initial vibrational state.

The time-dependent density distribution along the reaction coordinate is synthesized from the trajectories R_1, R_2, ..., R_N, using the *ansatz*[70]

$$\rho(R_i) = \frac{1}{N(R_{i+1} - R_i)} \tag{4}$$

The function $\rho(R_i)$ approaches the exact quantum mechanical density distribution in the limit $N \rightarrow \infty$. In section III, we show that numerically converged results can be obtained for a relatively small number of interacting trajectories ($N = 250$).

The time-dependent expectation value of a local operator $\hat{O}$ is evaluated by averaging over individual quantum trajectories:

https://doi.org/10.1021/acs.jpca.1c08678
J. Phys. Chem. A 2022, 126, 1805−1815

$$\langle \hat{O} \rangle(t) = \frac{1}{N} \sum_i O(R_i) \tag{5}$$

II.B. Numerical Details. For the evaluation of the vibrational eigenenergies and eigenstates along the r and R directions, the corresponding time-independent Schrödinger equation is solved using a Householder reduction algorithm with implicit shifts, as implemented in ref 77. Wave functions and operators are represented using finite-differences, on homogeneously spaced grids containing 2048 points and covering the ranges from r_{min} = 4.3 a_0 and r_{max} = 9.4 a_0 (for the Br−Br stretching), and from R_{min} = 6.1 a_0 and R_{max} = 14.3 a_0 (for the van der Waals mode).

Upon photoexcitation, trajectories were propagated during 120 ps. This value of the total simulation time was sufficient to compute the predissociation times for the range of initial vibrational levels explored here. The equations of motion of the canonical variables q_1, q_2, ..., q_{N_α}, p_1, p_2, ..., p_{N_α}, R_1, R_2, ..., R_N, P_1, P_2, ..., P_N, were solved using the fourth order Adams−Moulton predictor−corrector method with an adaptive time step and relative error tolerance of 10^{-10}. Upon modification of the time step size, we employed Nordsieck vectors[78,79] to compute a new equidistant sequence of previous state values using the new step size, in order to reinitialize the multistep integration. The overall integrator was started with the fourth order Runge−Kutta algorithm.

The (q_α, p_α) subspace comprises the generalized coordinates and conjugate momenta corresponding to the first N_α = 40 low-lying Br−Br vibrational states in the electronic state B. The time evolution of the canonical variables $q_\alpha(t)$, $p_\alpha(t)$ obeys the equations of motion (3), starting from the initial conditions: $q_\alpha(0) = \sqrt{2}\,\delta_{\alpha\nu}$, $p_\alpha(0) = 0$. This choice corresponds to the initial photoexcitation of the vibrational level ν of the Br_2 molecule. We simulated the vibrational predissociation of the $ArBr_2$ aggregates starting from the range of vibrational levels of the dihalogen with quantum numbers ν = 16 to ν = 25, on the potential energy surface corresponding to the B electronic state, for which experimental and wavepacket propagation results have been reported.[30]

The initial positions of the N = 250 quantum trajectories in the R direction were assigned using eq 4:

$$R_{i+1} = R_i + \frac{1}{N\rho_0(R_i)} \tag{6}$$

with i = 2, ..., N and R_1 = 6.7 a_0, where $\rho_0(R_i)$ represents the density distribution of the ground vibrational state along the van der Waals coordinate. The density $\rho_0(R_i)$ is vanishingly small at the starting position R_1, while the initial velocities of the quantum trajectories are all set to zero.

This number of trajectories was found to provide numerically converged results for the R-dependent observables. The residual unbalance between the interaction and the quantum forces, caused by the discretization of the initial density distribution along the van der Waals coordinate, is eliminated by the relaxation procedure described in refs 71 and 74.

III. RESULTS AND DISCUSSION

III.A. Vibrational Distributions. In Figure 1, we show the time-evolution of the vibrational distribution of the Br_2 molecule, for the $ArBr_2$ complexes initially excited to a vibrational eigenstate ν in the range from 16 to 25. It can be seen that the general trend of the vibrational population

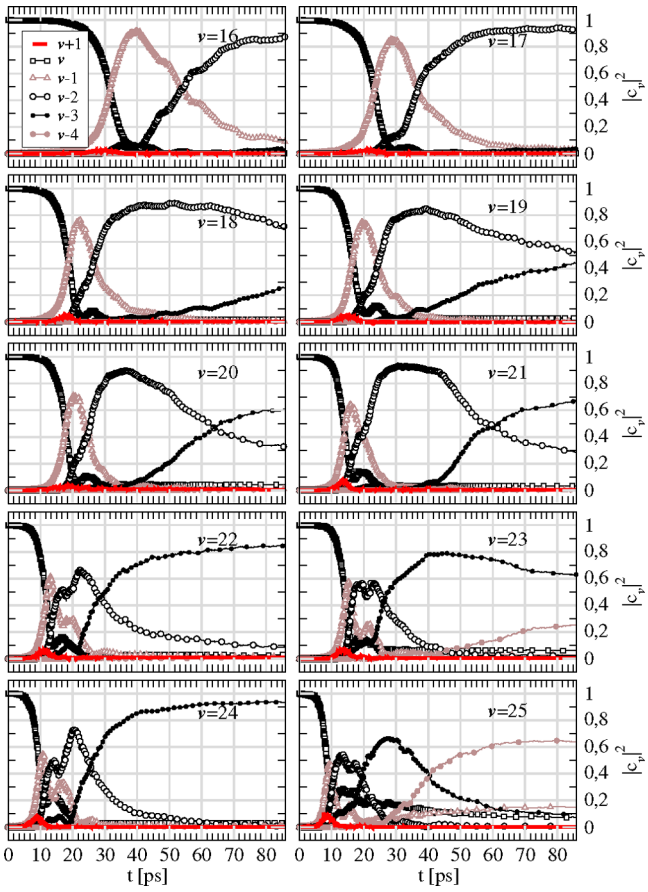

Figure 1. Time-dependent occupation probabilities of the vibrational levels in the range $\nu - 4$ to $\nu + 1$ of the Br_2 molecule, following the photoexcitation of the $ArBr_2(\nu)$ van der Waals complex.

dynamics is consistent with the picture of two oscillators, corresponding to the initial and final vibrational states of the Br_2 molecule, coupled indirectly with one or more secondary transient modes.

The triatomic complexes excited to the vibrational states ν = 16, 17, and 18, go through dissociation chiefly by transferring the energy corresponding to two vibrational quanta to the van der Waals mode. Likewise, the lost of three vibrational quanta is needed to break the van der Waals mode for initial excitations in the range from ν = 20 to ν = 24. The crossover from the $\nu' = \nu - 2$ to the $\nu' = \nu - 3$ dissociation channels occurs for the aggregates $ArBr_2(\nu$=19), which exhibit a sizable contribution of both product channels asymptotically. Furthermore, for the $ArBr_2(\nu$=25) complex, the $\nu - 4$ product state becomes the most probable dissociation channel for sufficiently long times. The transition between the initial and the final vibrational states is not a direct process, but one mediated by the transient population of intermediate quasi-bound states (most notably the level $\nu - 1$). The different decay pathways are explained later in this section.

The overall picture provided by the present simulations is consistent with the energetics of bond dissociation on the model potential energy surface used in this study, and it is in qualitative agreement with the experimental results and with the predictions of wavepacket propagation for the title system,[30] which allows to validate the effective phase space representation of the predissociation dynamics using the Hamiltonian of eq 2.

https://doi.org/10.1021/acs.jpca.1c08678
J. Phys. Chem. A 2022, 126, 1805−1815

The time-dependent vibrational populations displayed in Figure 1 exhibit a nonexponential decay of the initial vibrational state, in particular, the presence of a finite time delay $\tau_0(\nu)$ before the onset of the vibrational energy redistribution is striking. It can be seen that the time delay $\tau_0(\nu)$ gradually drops for increasing vibrational excitation. A similar plateau has been reported in QCT simulations of the vibrational predissociation dynamics of van der Waals complexes, and associated with a variety of factors (finite time required for the emitted atom(s) to reach the predetermined dissociation separation, continuous character of the intermode energy drift, zero-point energy violation, and presence of quasiperiodic trajectories, among others).[38,42] Conversely to QCT simulations, the origin of the time lag for dissociation, in the present quantum mechanical simulations, can be traced back to the implicit use of the TDH approximation (i.e., in the derivation of the Hamiltonian (2)).

As zeroth-order approximation, the predissociating complex can be considered as equivalent to two bilinearly coupled oscillators. Within first-order perturbation theory, the transition amplitude to the vibrational state with quantum number n is given by[80]

$$c_{n\nu} = -\frac{i}{\hbar}\int_0^t dt'\, e^{i\omega_{n\nu}t'} V_{n\nu}^{(TDH)}(t') = -\frac{i}{\hbar}\int_0^t dt'\, e^{i\omega_{n\nu}t'}[V_{n\nu}(t') - \Delta_{n\nu}(t')], \quad (7)$$

where $V_{n\nu}$ and $V_{n\nu}^{(TDH)}$ stand for the coupling matrix elements within the full dimensional and the TDH descriptions, respectively, whereas $\Delta_{n\nu}$ are the matrix elements of the function $\Delta(r, R) = \kappa(r - \langle r\rangle)(R - \langle R\rangle)$. κ is the bilinear coupling constant, $\langle r\rangle$ and $\langle R\rangle$ represent the time-dependent expectation values of the Jacobi coordinates r and R, respectively.

The initial wave function consists in the product of single-particle functions, corresponding to energy eigenstates along the coordinates r and R. Since these eigenstates are spatially delocalized, the error term $\Delta(r,R)$ introduced by the TDH *ansatz* is non negligible. In eq 7, the two terms inside the brackets partially cancel each other during the early dynamics, leading to smaller vibrational relaxation rates compared to the full dimensional description.

As vibrational transitions and intermode energy flow occur, the wave function evolves into a superposition of vibrational states, both for the diatomic stretching and for the van der Waals mode. As a consequence, the width of the time-dependent density distribution narrows down along the r and R directions, and the Jacobi coordinates become nearly constant over the interval where the time-dependent density distribution is non negligible, thereby reducing the size of the TDH error term. Detailed investigations on the accuracy of the TDH approximation in the photodissociation and on the vibrational predissociation dynamics of dihalogen−rare gas complexes and on its relevance for different regions of the diatom−rare gas interaction potential have been reported elsewhere.[81−84]

In the remainder of this section, we will show that adding the time lag $\tau_0(\nu)$, to the lifetimes computed via the fitting of the exponentially decaying part of the population dynamics, brings the predissociation rates computed within the ITR in close agreement with experimental results.

Within the present model, for every initial state ν, the early vibrational deactivation dynamics mainly consists in the loss of one vibrational quantum ($\nu \rightarrow \nu - 1$), and the subsequent loss of one additional quantum ($\nu - 1 \rightarrow \nu - 2$) once the occupation probability of the ν vibrational level reaches a threshold value of about 0.4. Additional Br−Br vibrational decay occurs for the higher excited van der Waals complexes (i.e., $\nu \geq 18$).

This predominant decay route competes with other relaxation pathways, such as the transient population of the $\nu + 1$ vibrational level, followed by the sequential loss of one vibrational quantum. Analogously, after the population of the vibrational state $\nu - 1$ reaches its maximum, the occupation of this level decays not only by populating the $\nu - 2$ level, but also the ν state (to a much lesser extent). Hence, the vibrational predissociation dynamics of the T-shaped $ArBr_2$ complexes involves at least three different decay pathways (i.e., the $\nu \rightarrow \nu - 1 \rightarrow \nu - 2 \rightarrow \cdots$, $\nu \rightarrow \nu + 1 \rightarrow \nu \rightarrow \nu - 1 \rightarrow \cdots$, and $\nu \rightarrow \nu - 1 \rightarrow \nu \rightarrow \nu - 1 \rightarrow \cdots$ channels). The interference of these decay paths also causes deviations of the time-dependent vibrational populations in Figure 1 from the simple exponential behavior.

As larger values of the energy deposited by the laser in the Br−Br stretching mode are considered, the energy spacing among the vibrational levels gets smaller in the neighborhood of the one initially excited. As a consequence, the overlap between the corresponding vibrational eigenfunctions increases, leading to larger coupling matrix elements $W_{\alpha\alpha'}$. Therefore, the vibrational energy redistribution occurs faster, and the height of the peak in the occupation probability of the level $\nu - 1$ shifts downward (i.e., it depletes monotonously from 92% for the predissociation of the $ArBr_2(\nu{=}16)$ aggregate, down to 47% for the $ArBr_2(\nu{=}25)$ complex).

Noteworthy, the fractional excitation of the neighboring more excited vibrational level $\nu + 1$ takes place for each initial state ν (see Figure 2), reflecting the energy drain from the van

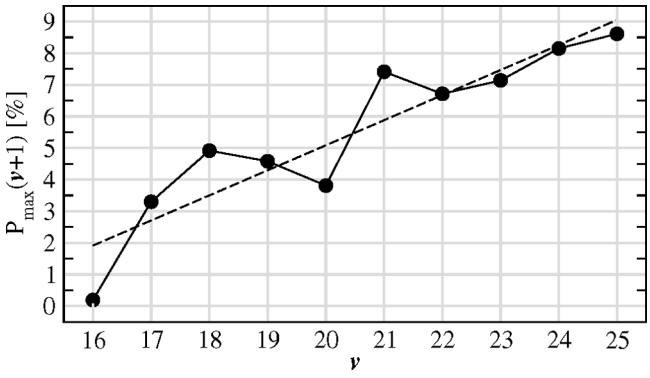

Figure 2. Maximum occupation probabilities (in percentage) of the vibrational level $\nu + 1$ of the Br_2 molecule, upon photoexcitation of the $ArBr_2(\nu)$ van der Waals complex. The straight line providing the best fit of the $P_{max}(\nu + 1)$ data is included to guide the eye.

der Waals mode into the Br_2 stretching mode at early stages of the vibrational energy redistribution process. The maximum occupation probability of the $\nu + 1$ level, P_{max}, increases roughly linearly with the vibrational quantum number ν.

In Figure 3, we show the lifetime $\tau(\nu)$ of the predissociating triatomic complexes $ArBr_2(\nu{=}16,...,25)$, as a function of the initial vibrational level ν. The predissociation time $\tau(\nu)$ is computed by fitting the total, time-dependent occupation

https://doi.org/10.1021/acs.jpca.1c08678
J. Phys. Chem. A 2022, 126, 1805−1815

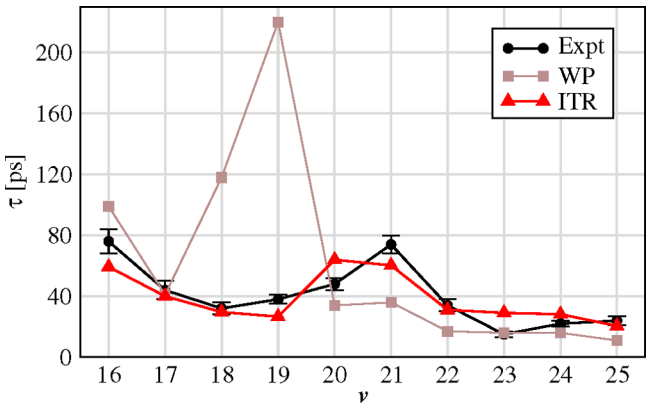

Figure 3. Lifetimes of the predissociating $ArBr_2(B,\nu)$ van der Waals complexes: effective phase space dynamics (up triangles), wavepacket propagation (squares[30]), and experiment (circles[30]).

probability of the ensemble of final vibrational states to single exponential rise functions, and adding the delay time $\tau_0(\nu)$, as described in section II.

It can be seen that the rate of vibrational deactivation is not a monotonous function of the initial vibrational quantum number. This is a fingerprint of the intramolecular vibrational energy redistribution that takes place upon photoexcitation. The larger the initial excess energy deposited in the Br−Br stretching mode, the stronger the coupling of the initially excited mode with the remaining degrees of freedom. Therefore, the initial state evolves in a coherent superposition of vibrational levels eventually leading to the dissociation of the complex.

Previous three-dimensional wavepacket calculations of the predissociation of $ArBr_2$ aggregate (for instance, upon photoexcitation of the vibrational level $\nu = 15$) have shown that the wavepacket, initially confined to the T-shape geometry, spreads over the entire range of possible relative orientations between the Jacobi vectors (see Figure 7 in ref 30). However, the overall correspondence between the predissociation times predicted by the present trajectory-based model and the corresponding experimental results indicates that the widening of the angular distribution has a mild impact on the lifetime of the triatomic complex.

It can be noticed that the lifetimes $\tau(\nu)$, computed within the effective phase space representation, deviate the most from the corresponding experimental values in the vicinity of level $\nu = 20$. The latter is the smallest Br−Br vibrational quantum number for which the loss of three vibrational quanta is needed in order to trigger the dissociation. Laying at the energy threshold of the $\Delta\nu = -2$ channel renders the dynamical evolution of the $ArBr_2(B,\nu)$, $\nu = 19$, 20, and 21, complexes very sensitive to the specific values of the parameters of the model potential energy surface.

In general, the lifetimes computed within the present trajectory based framework are in qualitative agreement with experimental measurements carried out for the $ArBr_2(B,\nu)$ aggregates. Some of the approximations included in the present model (most notably, the dimensionality reduction, and the underlying TDH approximation) hinder a direct comparison with the results of wavepacket propagation in ref 30. Other aspects, such as the contributions of other rotational states (i.e., for nonzero total angular momentum), or the ratio between vibrational and electronic predissociation rates, may also limit the correspondence between experimental values and the present theoretical estimates. For example, higher rotational states can be populated as a consequence of changing the gas mixture expansion conditions, and different rotational states may undergo distinct predissociation dynamics.[30] In spite of these approximations, the predictions of the present methodology are competitive with those of wavepacket propagation. The level of correspondence observed in Figure 3, supports the adequacy of the present two-dimensional phase space model to capture the essentials of the vibrational predissociation of T-shaped $ArBr_2$ complexes.

III.B. Time-Dependent Density Distribution. The time-dependent reduced density along the reaction coordinate, $\rho(R,t)$, was synthesized from the time evolution of the interacting trajectories $R_1(t)$, $R_2(t)$, ..., $R_N(t)$. As illustrative examples, the density distribution $\rho(R,t)$ is displayed in Figure 4 for the initial vibrational levels $\nu = 20$ and $\nu = 25$. They

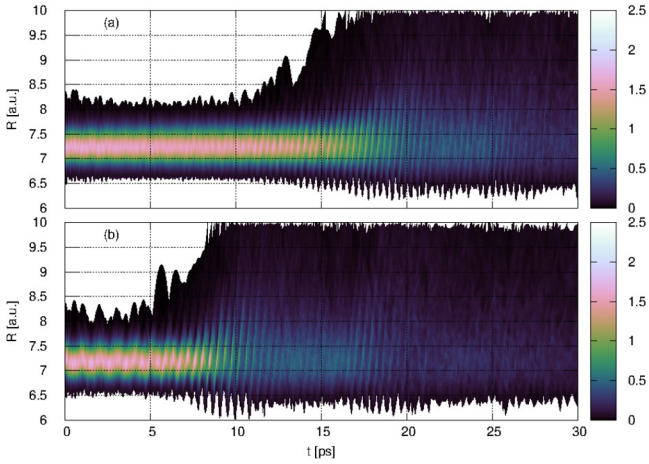

Figure 4. Predissociation dynamics: time-evolution of the density distribution along the van der Waals mode, following the initial excitation of the vibrational states (a) $\nu = 20$ and (b) $\nu = 25$ of the Br_2 molecule.

correspond, respectively, to the initial states exhibiting the overall slowest and fastest predissociation dynamics (i.e., the initial quantum numbers $\nu = 20$ and $\nu = 25$ constitute, separately, the global maximum and the global minimum in the $\tau(\nu)$ curve computed in the interacting trajectories framework).

In spite of the differences in the lifetime of the van der Waals aggregate, the density distribution dynamics reveals that the predissociation mechanism is similar in every case. At first, the mild differences between the van der Waals interaction potentials in the X and in the B electronic states cause a minor reorganization of the density distribution. From the onset of the vibrational deactivation of the Br_2 molecule, after approximately 10 ps (5 ps) since the photoexcitation of the $\nu = 20$ ($\nu = 25$) vibrational level, the width of the reduced density $\rho(R, t)$ increases gradually. The broadening of the density distribution causes an increase of the probability at short Ar−Br_2 distances. The chief effect of the atoms drawing nearer is the enhancement of the energy transfer from the Br_2 stretching into the motion along the van der Waals mode, thereby enhancing dissociation.

On the one hand, as a result of the larger extent of the vibrational energy redistribution prior to dissociation, the density of $ArBr_2$ corresponding to level $\nu = 25$ peaks more strongly than that of the level $\nu = 20$. Concomitantly, the time

https://doi.org/10.1021/acs.jpca.1c08678
J. Phys. Chem. A 2022, 126, 1805−1815

evolution of the position of the main peak (of the former distribution) mimics that of a classical oscillator more closely. On the other hand, it can be noticed that the detachment of the rare gas atom does not occur in a single step; instead, it takes many oscillations and successive splittings of the main density distribution at the outer turning point, eventually leading to the fragmentation of the $ArBr_2$ complex.

III.C. Phase Space Dynamics. One of the appealing features of the trajectory-based formulation is the possibility to analyze dynamical phenomena via its time evolution in phase space. This allows to gain insight, for example, on the mechanisms underlying the dissociation for the triatomic aggregates for which the present theoretical calculations over- or underestimate the lifetime of the complex (with respect to the experimental predissociation times).

In the following, we will focus on the vibrational predissociation dynamics of the $ArBr_2(B,\nu)$ aggregates in the vicinity of the threshold between the $\Delta\nu = -2$ and $\Delta\nu = -3$ dissociation channels.

Figure 5 displays the trajectory picture of the predissociating dynamics using two-dimensional cuts of the configuration

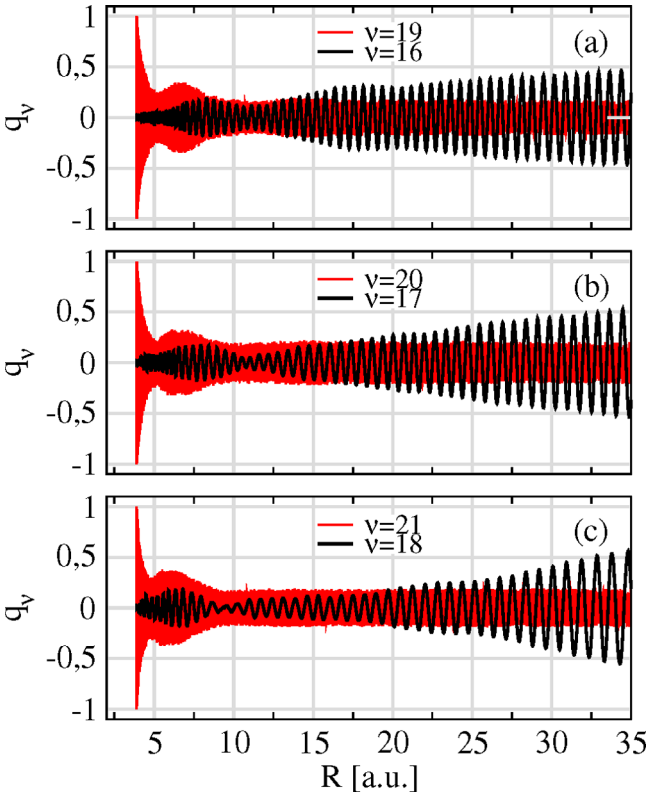

Figure 5. Coordinates q_ν and $q_{\nu-3}$, as a function of the van der Waals distance R, corresponding to the initial excitation of the vibrational levels $\nu = 19$ (top panel), $\nu = 20$ (middle panel), and $\nu = 21$ (bottom panel) of the Br_2 molecule.

space. It shows the R-dependence of the amplitude of the q_α modes associated with the initial and final vibrational states of the diatomic molecule, for the excitation of the states $\nu = 19$, 20, and 21, and for the predissociation channel $\Delta\nu = -3$. Upon photoexcitation of each vibrational state ν, the initially excited modes q_ν perform oscillations with the same frequency (6.3 ps^{-1}, which is roughly six times larger than the frequency of the early oscillations of the van der Waals coordinates R_i). The subsequent energy transfer to neighboring vibrational modes $q_{\alpha\neq\nu}$ cause the shift of the oscillation frequency of the coordinate q_ν. Intuitively, as a general trend, the amplitude of the oscillations of the coordinates q_ν and $q_{\nu-3}$ gets smaller and larger, respectively, as the density distribution moves outward along the van der Waals coordinate R.

Moreover, Figure 5 points to the configurational origin of the relatively slower predissociation of the $ArBr_2(\nu=20)$ and the $ArBr_2(\nu=21)$ aggregates. At short separations between the Ar atom and the Br_2 molecule, the amplitude of the q_ν oscillations gets depleted as the probability density moves in the direction of increasing R. Nevertheless, at intermediate distances in the R direction, the fractional enlargement of q_ν amplitude is favored. It can be noticed that the R-dependence of the vibrational couplings results in regions where the population of the $\Delta\nu = -3$ dissociation channel is markedly depleted. This behavior is more pronounced in the case of the initial excitation of the vibrational levels $\nu = 20$ and $\nu = 21$, whereas this is not the case in the dissociation of the $ArBr_2(\nu=19)$ complex. As a consequence, the dissociation of the $ArBr_2(\nu=20)$ and $ArBr_2(\nu=21)$ aggregates is inhibited by the partial repopulation of bound vibrational channels, as the portion of the density in the region of the van der Waals potential well moves outward.

The time evolution of the interacting trajectories upon excitation of the initial vibrational states with quantum numbers $\nu = 19$, 20, and 21 is plotted in Figure 6, together with the coordinates $q_\nu(t)$ and $q_{\nu-3}(t)$ corresponding to the initial state and to the most probable final vibrational state, respectively.

It can be seen that conversely to the early dynamics along the q_ν modes, the coordinates corresponding to the final vibrational states exhibit quite different oscillation frequencies (i.e., the larger the quantum number of the dissociation channel, the larger the vibrational period). Such differences reflect the different degrees of coupling among the q_ν degrees of freedom resulting from the predissociation dynamics.

The exit times of the interacting trajectories (roughly defined as the time it takes the trajectories to surpass the limits of the van der Waals interaction region, ~10 a_0) are broadly distributed along the ordinate-axis, resulting in significant spread of the probability density. Moreover, the centroid of the density distribution abandons the interaction region 21, 22, and 18.3 ps, respectively, after the photoexcitation of the $\nu = 19$, 20, and 21 vibrational levels of the Br_2 molecule. These exit times are between 21% and 70% smaller compared to the lifetime of the corresponding $ArBr_2(B,\nu)$ complexes. Therefore, the centroid of the probability distribution itself does not provide a precise estimation of the dissociation time, and accounting for quantum delocalization is a prerequisite for the correct description of the predissociation mechanism of the target system.

At the same time, for every initial state in Figure 6, the early decay of the amplitude of the q_ν oscillatory mode takes place before the $q_{\nu-3}$ mode becomes active. This behavior is reminiscent of the reaction proceeding via a cascade of transitions between neighboring vibrational states (cf. Figure 1). Within the effective phase space representation, the intermode coupling causes the energy redistribution among a handful of degrees of freedom belonging to the q_ν subspace. Notwithstanding the chiefly unidirectional character of this redistribution, Figure 6 shows that the energy actually flows back and forth between the coupled modes. This is consistent

https://doi.org/10.1021/acs.jpca.1c08678
J. Phys. Chem. A 2022, 126, 1805−1815

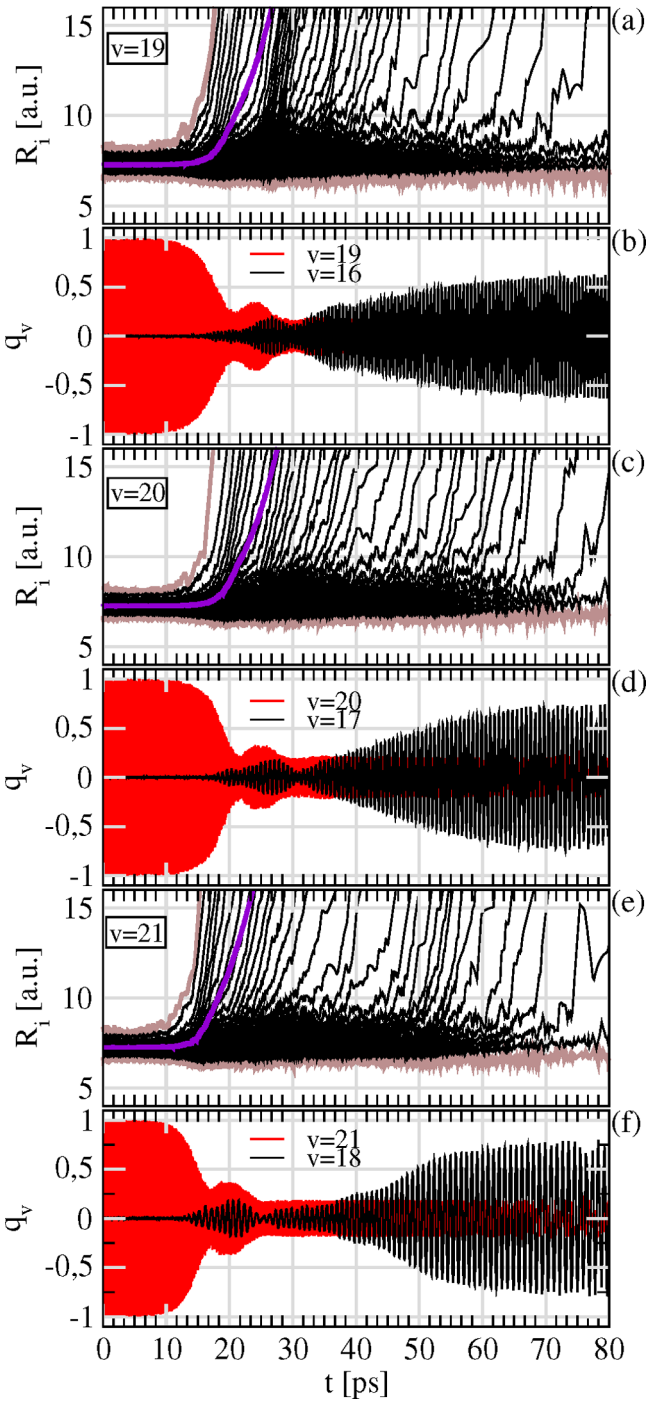

Figure 6. Time evolution of the interacting trajectories R_1, R_2, ..., R_N, and of the oscillation modes q_ν and $q_{\nu-3}$, corresponding to the initial excitation of the vibrational levels ν = 19 (top panels: a and b), ν = 20 (middle panels: c and d), and ν = 21 (bottom panels: e and f) of the Br_2 molecule. In panels a, c, and e, the inner- and outermost interacting trajectories, R_1 and R_N, are shown in brown, whereas the violet curve represents the time evolution of the centroid of the probability distribution.

with the molecular wave function being a coherent superposition of vibrational states.

Figure 7 depicts the total energy distribution along the reaction coordinate, for selected time intervals, and after the photoexcitation of the $ArBr_2$(B,ν=16) and $ArBr_2$(B,ν=25) aggregates. It exemplifies the redistribution mechanism, among

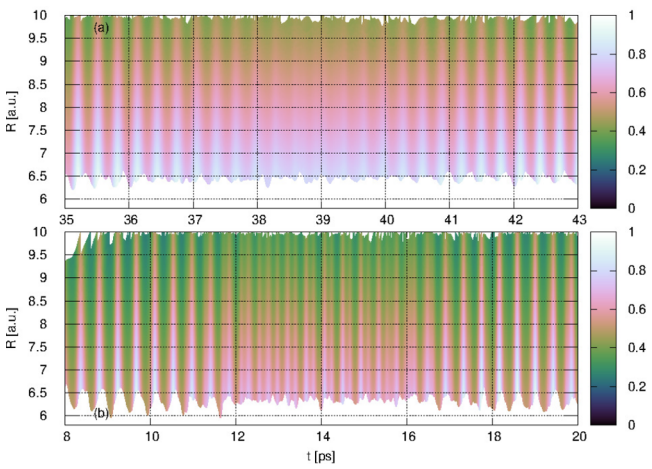

Figure 7. Total energy of the interacting trajectories (in atomic units) along the reaction coordinate R, (a) between 35 and 43 ps after the photoexcitation of the vibrational level ν = 16 of the diatomic molecule and (b) between 8 and 20 ps after the photoexcitation of the vibrational level ν = 25.

the interacting trajectories, of the energy transferred from the Br−Br stretching mode. It can be observed that the inner trajectories experience the larger energy gain while they visit the highly repulsive region of the van der Waals potential, during the expansion phase of the probability distribution breathing. Likewise, reshuffling of the excess energy leads to two possible scenarios:

(i) The set of interacting trajectories that remain bound can successfully accommodate the extra energy picked up during a first collision with the diatomic molecule, i.e., no significant rise occurs in the average energy of the outermost trajectories (e.g., between 38 and 40 ps after the photoexcitation of $ArBr_2$(B,ν = 16), and between 12 and 14 ps after photoexcitation of $ArBr_2$(B,ν = 25)). During this period, no further increase of the population of the exit dissociative channel occurs ($\Delta\nu$ = −2 and $\Delta\nu$ = −3, for the initial excitation of the vibrational levels ν = 16 and ν = 25, respectively).

(ii) The excess energy propagates outward along the chain of interacting trajectories, and the bound portion of the density distribution stabilizes by emitting one or more trajectories.

Conversely to other trajectory-based approaches to vibrational predissociation such as the QCT method (where every dissociative trajectory increases its energy beyond the dissociation limit), here the excess energy is transmitted along the reaction coordinate, and only the outermost trajectories get dissociated. This is a consequence of the noncrossing rule obeyed by the quantum trajectories, and that is strictly abided in the numerical implementations of the ITR. Although the details of the dissociation mechanism (i.e., how many collisions take place between dissociation events, how many interacting trajectories are emitted in every cycle) depend on the specific initial vibrational state of the van der Waals aggregate, the overall picture remains similar for all the predissociating complexes investigated.

IV. CONCLUSIONS

We studied the vibrational predissociation of T-shaped $ArBr_2$(B,ν) van der Waals complexes within a trajectory-

https://doi.org/10.1021/acs.jpca.1c08678
J. Phys. Chem. A 2022, 126, 1805−1815

based formulation. The fully quantum mechanical formalism enables one to represent the time evolution of the predissociation process in terms of trajectories evolving in an extended phase space. The initial assessment of the performance of the 2-fold mapping of the quantum dynamics of vibrational predissociation, carried out in ref 74, was extended here to span the range of experimentally accessible initial conditions,[30] and it was shown to cope with markedly different predissociation mechanisms.

In particular, the lifetimes of the predissociating complexes predicted by the present approach show that the method is competitive with wavepacket propagation techniques. For the initial vibrational states that are energetically closer to the threshold between the $\Delta\nu = -2$ and $\Delta\nu = -3$ predissociation channels (i.e., for the vibrational quantum numbers $\nu = 19$, 20, and 21), the agreement is less satisfactory. Nevertheless, taking into account the assumptions made in the numerical simulations (e.g., vanishing total angular momenta, constraining to the T-shape geometry, model pairwise potential energy surface), this level of correspondence can be considered as sufficiently good.

The present calculations confirmed that the competition between several simultaneous vibrational relaxation pathways has a direct impact on the predissociation dynamics. The analysis of the time evolution of the trajectories revealed the existence of regions of the effective phase space where transitions to vibrational states of higher energy are more likely to occur. The size and the location of these regions influences the transient vibrational distributions and therefore the computed lifetimes.

One of the attractive features of the present formulation is the possibility to simulate quantum phenomena (e.g., incorporating quantum delocalization and interference) in a trajectory framework. Specifically, quantum effects along the dissociation coordinate are mimicked by first and second nearest neighbors interactions. This results in a Hamiltonian description of the dynamics which is local in the effective phase space R_1, R_2, ..., R_N, P_1, ..., P_N, which is very appealing regarding the application of the formalism to the simulation of vibrational predissociation of larger aggregates.

Regarding computational efficiency, the cost of the Interacting Trajectory Representation is dominated by the evaluation of the quantum force (i.e., of nearest neighbor interactions). Thus, the numerical effort scales linearly with the number of trajectories. Furthermore, quantum trajectories only sample the regions where the probability density is non-negligible. Therefore, the number N of trajectories required to sample the probability distribution along each degree of freedom approaches the optimal number of basis functions or grid points that would be needed in a traditional wavepacket calculation (in order to achieve the same precision). Hence, the computational effort of the multidimensional ITR of quantum dynamics, for a d-dimensional system ($\sim N^d$), would be at least comparable to that of state-of-the-art multidimensional wavepacket propagation techniques such as the Multi-Configurational Time-Dependent Hartree method.[80,88]

The extension of the present model to investigate aggregates involving a dihalogen-molecule and several adatoms is conceptually straightforward, and it is only limited by the numerical challenge of propagating quantum trajectories in multidimensional spaces. The method could be applied also to systems where the separation between "fast" and "slow" modes is not so pronounced. The projection on the eigenstates of the Hamiltonian of the "fast" subsystem is formally equivalent to the adiabatic separation in electronic structure theory, and the methods developed over the years to tackle nonadiabatic dynamics in a quantum trajectory framework are also applicable in the context of the classical-like representation of quantum dynamics. Separated sets of quantum trajectories (with time-dependent weights) can be assigned for each eigenstate, augmented by standard techniques to circumvent singularities in the interstate quantum potential.[85−87] Other choices, such as mixed coordinate/polar wave function representations are also applicable.[86,87]

Moreover, the mapping into an equivalent classical-like system (comprising both high-frequency oscillatory modes and the interacting trajectories) paves the way for the development of further approximate methods. For example, the reduction of dimensionality by integrating over the set of comparably faster degrees of freedom would extend significantly the domain of applicability of the present model, especially to treat larger van der Waals clusters.

AUTHOR INFORMATION

Corresponding Author

Llinersy Uranga-Piña − *Laboratoire Collisions Agrégats Réactivité (IRSAMC), UMR 5589, Université Toulouse III - Paul Sabatier, F-31062 Toulouse Cedex 09, France; DynAMoS (Dynamical Processes in Atomic and Molecular Systems), Facultad de Física, Universidad de la Habana, Havana 10400, Cuba;* orcid.org/0000-0001-5837-7204; Email: llinersy@gmail.com

Authors

Juan Carlos Acosta-Matos − *Department of Physics, Centre for Technological Applications and Nuclear Developments (CEADEN), Havana 11300, Cuba*

Christoph Meier − *Laboratoire Collisions Agrégats Réactivité (IRSAMC), UMR 5589, Université Toulouse III - Paul Sabatier, F-31062 Toulouse Cedex 09, France*

Aliezer Martínez-Mesa − *Laboratoire Collisions Agrégats Réactivité (IRSAMC), UMR 5589, Université Toulouse III - Paul Sabatier, F-31062 Toulouse Cedex 09, France; DynAMoS (Dynamical Processes in Atomic and Molecular Systems), Facultad de Física, Universidad de la Habana, Havana 10400, Cuba*

Complete contact information is available at: https://pubs.acs.org/10.1021/acs.jpca.1c08678

Notes

The authors declare no competing financial interest.

ACKNOWLEDGMENTS

The results incorporated in this publication have received funding from the European Union's Horizon 2020 research and innovation programme under the Marie Sklodowska-Curie Grant Agreement No. 898663. This study has been partially supported through the EUR grant NanoX n ANR-17-EURE-0009 in the framework of the Programme des Investissements d'Avenir. The work was partially supported by the Abdus Salam International Centre of Theoretical Physics within its Associate Scheme (A.M.-M.) and Visitor Program (L.U.-P.). L.U.-P. thanks the HPC Service of ZEDAT, Freie Universität Berlin, for computing time.

REFERENCES

(1) Vendruscolo, M.; Dobson, C. M. Protein Dynamics: Moore's Law in Molecular Biology. *Curr. Biol.* **2011**, *21*, R68.
(2) Rahimian, A.; et al. *Proceedings of the 2010 ACM/IEEE International Conference for High Performance Computing, Networking, Storage and Analysis, New Orleans, LA*; 2010; pp 1−11.
(3) Germann, T. C.; Kadau, K. Trillion atom molecular dynamics becomes reality. *Int. J. Mod. Phys. C* **2008**, *19*, 1315.
(4) Eckhardt, W.; et al. 591 TFLOPS Multi-trillion Particles Simulation on SuperMUC. *Lecture Notes in Computer Science* **2013**, *7905*, 1.
(5) Janda, K. C. Predissociation of Polyatomic Van Der Waals Molecules. *Advances in Chemical Physics* **2007**, *60*, 201.
(6) Rohrbacher, A.; Williams, J.; Janda, K. C. Rare gas-dihalogen potential energy surfaces. *Phys. Chem. Chem. Phys.* **1999**, *1*, 5263.
(7) Gonzalez-Lezana, T.; Hernández, M. I.; Delgado-Barrio, G.; Buchachenko, A. A.; Villarreal, P. Vibrational predissociation dynamics of the $He^{79}Br_2$ van der Waals molecule: A quantum mechanical study. *J. Chem. Phys.* **1996**, *105*, 7454.
(8) Roncero, O.; Caloto, D.; Janda, K. C.; Halberstadt, N. From the sparse to the statistical limit of intramolecular vibrational redistribution in vibrational predissociation: $ArCl_2$ as an example. *J. Chem. Phys.* **1997**, *107*, 1406.
(9) Willberg, D. M.; Gutmann, M.; Breen, J. J.; Zewail, A. H. Real-time dynamics of clusters. I. I_2X_n (n = 1). *J. Chem. Phys.* **1992**, *96*, 198.
(10) Beswick, J. A.; Halberstadt, N.; Janda, K. C. Structure and dynamics of noble gas-halogen and noble gas ionic clusters: When theory meets experiment. *Chem. Phys.* **2012**, *399*, 4.
(11) Valdes, A.; Prosmiti, R.; Villarreal, P.; Delgado-Barrio, G.; et al. Ab initio vibrational predissociation dynamics of He-I_2(B) complex. *J. Chem. Phys.* **2007**, *126*, 244314.
(12) Boucher, D. S.; Loomis, R. A. Stabilization of Different Conformers of Weakly Bound Complexes to Access Varying Excited-State Intermolecular Dynamics. *Advances in Chemical Physics* **2008**, *138*, 375.
(13) Gray, S. K.; Wozny, C. E. Fragmentation mechanisms from three-dimensional wave packet studies: Vibrational predissociation of $NeCl_2$, $HeCl_2$, NeICl, and HeICl. *J. Chem. Phys.* **1991**, *94*, 2817.
(14) Garcia-Vela, A.; Henriksen, N. E. Unravelling the role of quantum interference in the weak-field laser phase modulation control of photofragment distributions. *Phys. Chem. Chem. Phys.* **2016**, *18*, 4772.
(15) Garcia-Vela, A. Highly delocalized orbiting resonances. *J. Chem. Phys.* **2008**, *129*, 094307.
(16) Halberstadt, N.; Beswick, J. A.; Schinke, R. Rotation distributions in the vibrational predissociation of weakly bound complexes: Quasi-classical golden rule treatment. *AIP Conf. Proc.* **1990**, *225*, 211.
(17) Buchachenko, A. A.; Stepanov, N. F.; Krems, R. V.; Nordholm, S. Vibrational predissociation of ArHF: a test of global semiempirical potential energy surfaces. *Phys. Chem. Chem. Phys.* **2002**, *4*, 4992.
(18) Valdes, A.; Prosmiti, R. Quantum vibrational dynamics of the Ar_2ICl cluster. *Europe Phys. J. D* **2016**, *70*, 3.
(19) Zhang, D. H.; Zhang, J. Z. H.; Bačić, Z. A time-dependent golden rule wave packet calculation for vibrational predissociation of D_2HF. *J. Chem. Phys.* **1992**, *97*, 927.
(20) Borowski, A.; Kuhn, O. Nonadiabatic quantum dynamics of Br_2 in solid Ar: A four-dimensional study of the B to C state predissociation. *Chem. Phys.* **2008**, *347*, 523.
(21) Stephenson, T. A.; Halberstadt, N. Quantum calculations on the vibrational predissociation of $NeBr_2$: Evidence for continuum resonances. *J. Chem. Phys.* **2000**, *112*, 2265.
(22) Roncero, O.; Beswick, J. A.; Halberstadt, N.; Villarreal, P.; Delgado-Barrio, G. Photofragmentation of the Ne··· ICl complex: A three-dimensional quantum mechanical study. *J. Chem. Phys.* **1990**, *92*, 3348.
(23) Roncero, O.; Gray, S. K. Quantum dynamics of ArI_2 vibrational predissociation including low total angular momenta: The role of intramolecular vibrational energy redistribution. *J. Chem. Phys.* **1996**, *104*, 4999.
(24) Roncero, O.; Halberstadt, N.; Beswick, J. A. A three dimensional wave packet study of Ar···I_2(B) → Ar+I+I electronic predissociation. *J. Chem. Phys.* **1996**, *104*, 7554.
(25) Krause, P. J.; Clary, D. C. Vibrational predissociation of D_2HF and H_2HF with a new potential energy surface. *Mol. Phys.* **1998**, *93*, 619.
(26) Krause, P. J.; Clary, D. C. Time-dependent wavepacket study of the vibrational predissociation of He_2Br_2. *Phys. Chem. Comm.* **1999**, *2*, 5.
(27) Gray, S. K. Wave packet studies of the vibrational predissociation of three-and four-atom Van der Waals complexes. *Faraday Discuss.* **1994**, *97*, 143.
(28) Meier, C.; Manthe, U. Full-dimensional quantum study of the vibrational predissociation of the cluster. I_2··· Ne_2. *J. Chem. Phys.* **2001**, *115*, 5477.
(29) Taylor, M. A.; Pio, J. M.; van der Veer, W. E.; Janda, K. C. Competition between electronic and vibrational predissociation dynamics of the $HeBr_2$ and $NeBr_2$ van der Waals molecules. *J. Chem. Phys.* **2010**, *132*, 104309.
(30) Cabrera, J.; Bieler, C. R.; McKinney, N.; van der Veer, W. E.; Pio, J. M.; Janda, K.; Roncero, O. Time and frequency resolved dynamics of $ArBr_2$. *J. Chem. Phys.* **2007**, *127*, 164309.
(31) Villarreal, P.; Miret-Artes, S.; Roncero, O.; Delgado-Barrio, G.; Beswick, J. A.; Halberstadt, R.; Coalson, D. A wave packet Golden Rule treatment of vibrational predissociation. *J. Chem. Phys.* **1991**, *94*, 4230.
(32) Fang, J. Y.; Guo, H. Multiconfiguration time-dependent Hartree studies of the Cl_2Ne vibrational predissociation dynamics. *J. Chem. Phys.* **1995**, *102*, 1944.
(33) Krause, P. J.; Clary, D. C. The vibrational predissociation of $HeBr_2$: a wavepacket study. *Chem. Phys. Lett.* **1997**, *271*, 171.
(34) Halberstadt, N.; Serna, S.; Roncero, O.; Janda, K. C. Vibrational predissociation of the Ar···Cl_2 van der Waals complex: The small molecule limit for intramolecular vibrational redistribution. *J. Chem. Phys.* **1992**, *97*, 341.
(35) Halberstadt, N.; Beswick, A.; Roncero, O.; Janda, K. C. Intramolecular vibrational relaxation in a triatomic van der Waals molecule: $ArCl_2$. *J. Chem. Phys.* **1992**, *96*, 2404.
(36) Buchachenko, A.; Halberstadt, N.; Lepetit, B.; Roncero, O. Ar··· I_2: A model system for complex dynamics. *Int. Rev. Phys. Chem.* **2003**, *22*, 153.
(37) Woodruff, S. B.; Thompson, D. L. A quasiclassical trajectory study of vibrational predissociation of van der Waals molecules: Collinear He···I_2 ($B\ ^3\Pi$). *J. Chem. Phys.* **1979**, *71*, 376.
(38) González-Martínez, M. L.; Rubayo-Soneira, J.; Janda, K. Quasi-classical trajectories study of $Ne^{79}Br_2$ (B) vibrational predissociation. *Phys. Chem. Chem. Phys.* **2006**, *8*, 4550.
(39) Garcia-Vela, A.; Villarreal, P.; Delgado-Barrio, G. Dissociation dynamics of I_2 ··· Ne_n van der Waals clusters (n = 1−9): A quasiclassical approach. *J. Chem. Phys.* **1991**, *94*, 7868.
(40) Gray, S. K.; Rice, S. A.; Noid, D. W. The classical mechanics of vibrational predissociation: A model based study of phase space structure and its influence on fragmentation rates. *J. Chem. Phys.* **1986**, *84*, 3745.
(41) Alimi, R.; Garcia-Vela, A.; Gerber, R. B. A remedy for zero-point energy problems in classical trajectories: A combined semi-classical/classical molecular dynamics algorithm. *J. Chem. Phys.* **1992**, *96*, 2034.
(42) Garcia-Vela, A.; Rubayo-Soneira, J.; Delgado-Barrio, G.; Villarreal, P. Quasiclassical dynamics of the I_2···Ne_2 vibrational predissociation: A comparison with experiment. *J. Chem. Phys.* **1996**, *104*, 8405.
(43) Borrell-Grueiro, O.; Baños-Rodríguez, U.; Márquez-Mijares, M.; Rubayo-Soneira, J. Vibrational predissociation dynamics of the nitric oxide dimer. *Eur. Phys. J. D* **2018**, *72*, 121.
(44) González-Martínez, M. L.; Arbelo-González, W.; Rubayo-Soneira, J.; Bonnet, L.; Rayez, J. C. Vibrational predissociation of van

https://doi.org/10.1021/acs.jpca.1c08678
J. Phys. Chem. A 2022, 126, 1805−1815

der Waals complexes: Quasi-classical results with Gaussian-weighted trajectories. *Chem. Phys. Lett.* **2008**, *463*, 65.
(45) Mineo, H.; Lin, S. H.; Fujimura, Y. Adiabatic treatment for vibrational predissociation of water dimers with channel interactions. *J. Phys.: Conf. Ser.* **2015**, *635*, 112013.
(46) García-Vela, A. On the importance of an accurate representation of the initial state of the system in classical dynamics simulations. *J. Chem. Phys.* **2000**, *112*, 8302.
(47) García-Vela, A. An alternative phase-space distribution to sample initial conditions for classical dynamics simulations. *Chem. Phys.* **2002**, *285*, 245.
(48) Arbelo-González, W.; Bonnet, L.; García-Vela, A. *Phys. Chem. Chem. Phys.* **2013**, *15*, 9994.
(49) Sun, L.; Hase, W. L. New insights into the semiclassical Wigner treatment of photodissociation dynamics. *J. Chem. Phys.* **2010**, *133*, 044313.
(50) Rodríguez-Hernández, B.; Ondarse-Álvarez, D.; Oldani, N.; Martínez-Mesa, A.; Uranga-Piña, L.; Tretiak, S.; Fernández-Alberti, S. Modification of optical properties and excited-state dynamics by linearizing cyclic paraphenylene chromophores. *J. Phys. Chem. C* **2018**, *122*, 16639.
(51) Freixas-Lemus, V. M.; Martínez-Mesa, A.; Uranga-Piña, L. Quasi-classical trajectory study of atom-diatomic molecule collisions in symmetric hyperspherical coordinates: The F+HCl reaction as a test case. *J. Phys. Chem. A* **2016**, *120*, 2059.
(52) Uranga-Piña, L.; Martinez-Mesa, A.; Garcia-Reyes, L.; Rubayo-Soneira, J. Effective temperature representation of quantum delocalization effects on the dynamics of NO($A^2\Sigma^+ \leftarrow X^2\Pi^+$) photoexcitation in Ne matrices. *Phys. Chem. Chem. Phys.* **2009**, *11*, 5358.
(53) Martínez-Mesa, A.; Saalfrank, P. Semiclassical modelling of finite-pulse effects on non-adiabatic photodynamics via initial condition filtering: The predissociation of NaI as a test case. *J. Chem. Phys.* **2015**, *142*, 194107.
(54) Heller, E. J. Guided Gaussian wave packets. *Acc. Chem. Res.* **2006**, *39*, 127.
(55) Unn-Toc, W.; Uranga-Piña, L.; Meier, C.; Halberstadt, N.; Rubayo-Soneira, J. Quantum dynamics of solid Ne upon photo-excitation of a NO impurity: A Gaussian wave packet approach. *J. Chem. Phys.* **2012**, *137*, 054112.
(56) Akimov, A. V.; Prezhdo, O. V. Formulation of quantized Hamiltonian dynamics in terms of natural variables. *J. Chem. Phys.* **2012**, *137*, 224115.
(57) Prezhdo, O. V. Classical mapping for second-order quantized Hamiltonian dynamics. *J. Chem. Phys.* **2002**, *117*, 2995.
(58) Prezhdo, O. V.; Pereverzev, Y. V. Quantized Hamilton dynamics for a general potential. *J. Chem. Phys.* **2002**, *116*, 4450.
(59) Baytas, B.; Bojowald, M.; Crowe, S. Quantized Hamilton dynamics for a general potential. *Ann. Phys.* **2020**, *420*, 168247.
(60) Habershon, S.; Manolopoulos, D. E.; Markland, T. E.; Miller, T. F., 3rd Ring-polymer molecular dynamics: quantum effects in chemical dynamics from classical trajectories in an extended phase space. *Annu. Rev. Phys. Chem.* **2013**, *64*, 387.
(61) Briggs, J. S.; Eisfeld, A. Coherent quantum states from classical oscillator amplitudes. *Phys. Rev. A* **2012**, *85*, 052111.
(62) Briggs, J. S.; Eisfeld, A. Quantum dynamics simulation with classical oscillators. *Phys. Rev. A* **2013**, *88*, 062104.
(63) Meyer, H. D.; Miller, W. H. A classical analog for electronic degrees of freedom in nonadiabatic collision processes. *J. Chem. Phys.* **1979**, *70*, 3214.
(64) Wyatt, R. E. *Quantum dynamics with trajectories*; Springer Science & Business Media: 2006.
(65) Chattaraj, P. K. *Quantum Trajectories*; CRC Press/Taylor and Francis Group: 2010).
(66) Sanz, A. S.; Mirét-Artés, S. *A trajectory description of quantum processes. II. Applications*; Springer: 2014.
(67) Cruz-Rodriguez, L.; Tremblay, J. C.; Martinez-Mesa, A.; Uranga-Piña, L. A Chebyshev expansion of hydrodynamical fields for ultrafast wave packet dynamics. *Comput. Theor. Chem.* **2016**, *1078*, 104.
(68) Poirier, B. Bohmian mechanics without pilot waves. *Chem. Phys.* **2010**, *370*, 4.
(69) Schiff, J.; Poirier, B. Communication: Quantum mechanics without wavefunctions. *J. Chem. Phys.* **2012**, *136*, 031102.
(70) Hall, M. J.; Deckert, D. A.; Wiseman, H. M. Quantum phenomena modeled by interactions between many classical worlds. *Phys. Rev. X* **2014**, *4*, 041013.
(71) Cruz-Rodriguez, L.; Uranga-Pina, L.; Martinez-Mesa, A.; Meier, C. Quantum dynamics modeled by interacting trajectories. *Chem. Phys.* **2018**, *503*, 39.
(72) Cruz-Rodriguez, L.; Uranga-Pina, L.; Martinez-Mesa, A.; Meier, C. Quantum trajectory study of laser-driven atomic ionization. *Chem. Phys. Lett.* **2019**, *715*, 211.
(73) Donoso, A.; Martens, C. C. Quantum Tunneling Using Entangled Classical Trajectories. *Phys. Rev. Lett.* **2001**, *87*, 223202.
(74) Acosta-Matos, J. C.; Martinez-Mesa, A.; Uranga-Pina, L. Trajectory-based modelling of the quantum dynamics of vibrational predissociation: Application to the Ar-Br_2 (ν = 24) complex. *Chem. Phys.* **2020**, *529*, 110544.
(75) Buchachenko, A. A.; Baisogolov, A. Y.; Stepanov, N. F. Interaction potentials and fragmentation dynamics of the Ne-Br_2 complex in the ground and electronically excited states. *J. Chem. Soc. Faraday Trans.* **1994**, *90*, 3229.
(76) Pio, J. M.; van der Veer, W. E.; Bieler, C. R.; Janda, K. C. Product state resolved excitation spectroscopy of He-, Ne-, and Ar-Br_2 linear isomers: Experiment and theory. *J. Chem. Phys.* **2008**, *128*, 134311.
(77) Press, W. H.; Teukolsky, S. A.; Vetterling, W. T.; Flannery, B. P.; Metcalf, M. *Numerical Recipes in Fortran 90 - The Art of Parallel Scientific Computing*; Cambridge University Press: 1996.
(78) Nordsieck, A. On numerical integration of ordinary differential equations. *Math. Comp.* **1962**, *16*, 22.
(79) Butcher, J. C. Numerical methods for ordinary differential equations in the 20th century. *J. Comput. Appl. Math.* **2000**, *125*, 1.
(80) Beck, M. H.; Jäckle, A.; Worth, G. A.; Meyer, H. D. The multiconfiguration time-dependent Hartree (MCTDH) method: a highly efficient algorithm for propagating wavepackets. *Phys. Rep.* **2000**, *324*, 1.
(81) Garcia-Vela, A. Quantum dynamical study of I_2-Ne vibrational predissociation dynamics: A three-dimensional time-dependent self-consistent-field approach. *J. Chem. Phys.* **1996**, *104*, 1047.
(82) Bisseling, R. H.; Kosloff, R.; Gerber, R. B.; Ratner, M. A.; Gibson, L.; Cerjan, C. Exact time-dependent quantum-mechanical dissociation dynamics of I_2He: Comparison of exact time-dependent quantum calculation with two self-consistent field (TDSCF) approximations. *J. Chem. Phys.* **1987**, *87*, 2760.
(83) Garcia-Vela, A. On the validity of time-dependent self-consistent field approach: Application to the vibrational predissociation of Cl_2-Ne. *Chem. Phys. Lett.* **1998**, *290*, 155.
(84) Garcia-Vela, A. A test of the accuracy of the partially separable time-dependent self-consistent approach. *J. Chem. Phys.* **1999**, *111*, 8286.
(85) Wyatt, R. E.; Lopreore, C. L.; Parlant, G. Electronic transitions with quantum trajectories. *J. Chem. Phys.* **2001**, *114*, 5113.
(86) Rassolov, V. A.; Garashchuk, S. Semiclassical nonadiabatic dynamics with quantum trajectories. *Phys. Rev. A* **2005**, *71*, 032511.
(87) Garashchuk, S.; Rassolov, V. A. Modified quantum trajectory dynamics using a mixed wave function representation. *J. Chem. Phys.* **2004**, *121*, 8711.
(88) Meyer, H.-D., Gatti, F., Worth, G. A., Eds. *Multidimensional Quantum Dynamics: MCTDH Theory and Applications*; Wiley-VCH: 2009.

https://doi.org/10.1021/acs.jpca.1c08678
J. Phys. Chem. A 2022, 126, 1805−1815